Atmos. Chem. Phys., 23, 8979–8991, 2023
https://doi.org/10.5194/acp-23-8979-2023


Atmospheric Chemistry and Physics
Open Access
EGU

Research article

# Direct observation for relative-humidity-dependent mixing states of submicron particles containing organic surfactants and inorganic salts

**Chun Xiong[1,★], Binyu Kuang[1,★], Fei Zhang[1], Xiangyu Pei[1], Zhengning Xu[1], and Zhibin Wang[1,2]**

[1]Zhejiang Provincial Key Laboratory of Organic Pollution Process and Control, MOE Key Laboratory of Environment Remediation and Ecological Health, College of Environmental and Resource Sciences, Zhejiang University, Hangzhou 310058, China
[2]ZJU–Hangzhou Global Scientific and Technological Innovation Center, Zhejiang University, Hangzhou 311215, China
★These authors contributed equally to this work.

**Correspondence:** Zhibin Wang (wangzhibin@zju.edu.cn)

Received: 28 April 2023 – Discussion started: 4 May 2023
Revised: 13 July 2023 – Accepted: 14 July 2023 – Published: 11 August 2023

**Abstract.** Aerosol mixing state plays an important role in heterogeneous reactions and cloud condensation nuclei (CCN) activity. Organic surfactants could affect aerosol mixing state through bulk–surface partitioning. However, the mixing state of surfactant-containing particles remains unclear due to the lack of direct measurements. Here, direct characterizations of the mixing state for 20 kinds of submicron particles containing inorganic salts (NaCl and $(NH_4)_2SO_4$) and atmospheric organic surfactants (organosulfates, organosulfonates, and dicarboxylic acids) were conducted upon relative humidity (RH) cycling by environmental scanning electron microscopy (ESEM). As the RH increased, the surfactant shells inhibited water diffusion being exposed to the inorganic core, leading to notably increased inorganic deliquescence RH (88.3 %–99.5 %) when compared with pure inorganic aerosol. Meanwhile, we directly observed an obvious Ostwald ripening process (that is, the growth of larger crystals at the expense of smaller ones) in 6 out of 10 NaCl–organic surfactant systems. As a result of water inhibition by the organic surfactant shell, Ostwald ripening in all systems occurred at RH above 90 %, which were higher than the reported RH range for pure NaCl measured at 27 °C (75 %–77 %). As RH decreased, eight systems underwent liquid–liquid-phase separation (LLPS) before efflorescence, showing a strong dependence on the organic molecular oxygen-to-carbon ratio (O : C). Quantitatively, LLPS was always observed when O : C $\leq$ 0.43 and was never observed when O : C $>\sim$ 0.57. Separation RH (SRH) of inorganic salt–organic surfactant mixtures generally followed the trend of $(NH_4)_2SO_4$ < NaCl, which is consistent with their salting-out efficiencies reported in previous studies. Solid-phase separations were observed after efflorescence for systems without LLPS. Our results provide a unique insight into the consecutive mixing processes of the inorganic salt–organic surfactant particles, which would help improve our fundamental knowledge of model development on radiative effect.

Published by Copernicus Publications on behalf of the European Geosciences Union.

## 1 Introduction

Atmospheric particles are complex mixtures of multiple types of inorganic and organic matter (Pöschl, 2005). When relative humidity (RH) varies, particles can undergo phase transitions such as deliquescence (Peng et al., 2001), efflorescence (Takahama et al., 2007), and liquid–liquid-phase separation (LLPS; Martin, 2000), hence altering the mixing state. The transition of the aerosol mixing state can influence gas uptake, hygroscopicity, cloud condensation nuclei (CCN) activity, and radiative absorption (Riemer et al., 2019).

Upon hydration, previous studies have suggested that different mixing states between inorganic and organic matter influence aerosol hygroscopic behaviors (e.g., deliquescence) and solar radiation (Peng et al., 2016; Li et al., 2021). For instance, Peng et al. (2016) observed internal mixed NaCl–oxalic acid deliquesced at 73 % RH, which is slightly lower than that of pure NaCl (75 %) because of the interactions between inorganic and organic matter. However, Li et al. (2021) found a different deliquescence process if ammonium sulfate (AS) was coated by secondary organic aerosol; the organic shell first dissolved at $\sim$ 50 % RH, but the water uptake of the AS core was inhibited, leading to a higher deliquescence RH of AS ($\sim$ 83 %–90 %). Using cryogenic transmission electron microscopy (cryo-TEM), Zhang et al. (2022) directly observed collected particles from a rural site where the LLPS (inner inorganic phase and outer organic phase) between organic matter and inorganic salts remained when the RH was raised to between $75 \pm 2$ % and $86 \pm 2$ %, but the LLPS disappeared when the RH increased to $95 \pm 2$ %. They later suggested that LLPS with a higher ratio of organic coating thickness to the black carbon size can drive black carbon from an inorganic core to organic particle coatings, which could result in an 18 % radiative absorption overestimation of the black carbon aerosols in climate models when assuming a core shell particle structure.

Upon dehydration, a phase separation has been frequently observed in ambient particles (You et al., 2012; Ting et al., 2018; Zhang et al., 2020, 2022). For example, LLPS occurred at $>$ 90 % RH for particles containing the water extraction of collected atmospheric particles in Atlanta, GA, USA, and simulations indicated that LLPS can decrease the particle uptake of $N_2O_5$ and thus increase the concentrations of gas-phase $NO_3$ and $N_2O_5$ (You et al., 2012). Factors contributing to LLPS, such as oxidation levels (Bertram et al., 2011; Song et al., 2017, 2019), organic fraction (Ciobanu et al., 2009; Song et al., 2012a), inorganic species (You et al., 2013), and temperature (You and Bertram, 2015; Roy et al., 2020), have been discussed for some specific inorganic–organic or organic–organic systems in the literature. Song et al. (2012b) and You et al. (2013) found that LLPS always occurred for O : C $<\sim$ 0.5, never occurred for O : C $>$ 0.8, and when O : C was between 0.5 and 0.8, LLPS was depended on inorganic species. The organic fraction showed controversial effects on LLPS (Bertram et al., 2011; Song et al., 2012a), since Bertram et al. (2011) found a weak effect of organic fraction on LLPS for 8 out of 11 AS–organic systems, but the rest of the systems exhibited a quantifiable dependence of separation RH (SRH) on the organic fraction. You et al. (2013) reported that SRH values of inorganic organic mixed particles generally followed the trend of $(NH_4)_2SO_4 \geq NH_4HSO_4 \geq NaCl \geq NH_4NO_3$, which is consistent with inorganic salting-out efficiencies. Temperature did not strongly affect SRH between 253–290 K for AS–organic (O'Brien et al., 2015; You and Bertram, 2015) and NaCl–organic systems (Roy et al., 2020). Recently, the dry rate (Altaf and Freedman, 2017; Altaf et al., 2018) and size effect (Freedman, 2020; Ott and Freedman, 2021; Ohno et al., 2023) on LLPS were found for submicron particles. When undergoing drying through a fast rate ($\sim$ 27 % per minute), the phase separation of the AS–pimelic acid system occurred in larger particles (75–322 nm diameter), but smaller particles (below 25–135 nm diameter) were homogeneous. In slow drying rates (0.04 % to 0.08 % RH per second), particles with diameters below 43 nm were homogeneous, but larger particles (28–629 nm) were mainly phase-separated (Altaf and Freedman, 2017). Freedman (2020) further explained that LLPS scarcely occurs in smaller particles, as smaller particles cannot overcome the energy barrier needed to form a new phase.

Dicarboxylic acids (Ruehl and Wilson, 2014), organosulfates (Bruggemann et al., 2020; Reed et al., 2022), and organosulfonates (Bruggemann et al., 2020; Guo et al., 2020) are important organic constituents in secondary organic aerosol. Primary emission and secondary transition were major sources of dicarboxylic acids, and their mass contribution of dicarboxylic acids to total particulate carbon exceeds 10 % (Römpp et al., 2006; Ho et al., 2010; Hyder et al., 2012). Organosulfates and organosulfonates, as significant reservoirs of sulfur, comprise an estimated 5 %–30 % of the total organic aerosol mass (Tolocka and Turpin, 2012; Reed et al., 2022). The abovementioned organics contain both hydrophilic (e.g., sulfo group) and hydrophobic groups (e.g., alkyl group), showing surface activity and causing bulk–surface partitioning (Noziere, 2016; Ruehl et al., 2016), hence affecting individual aerosol morphology (Kwamena et al., 2010). However, the mixing state of submicron inorganic salt–organic surfactant particles remains unclear due to the lack of direct measurements. Here, we directly observed the mixing states of submicron particles containing inorganic salt and organic surfactant with a varying organic volume fraction (OVF) upon humidity cycling by environmental scanning electron microscopy (ESEM). Our results could provide unique insights into the dynamic evolution of inorganic salt–organic surfactant particles under fluctuating atmospheric conditions.

**Table 1.** Organic surfactants and their relevant properties investigated in this study.

| Species | Compounds | Formula | Solubility* ($mol\,L^{-1}$) | O : C | Purity | Supplier |
|---|---|---|---|---|---|---|
| Organic sulfonate | Sodium propane sulfonate | $C_3H_7SO_3Na$ | 2.5 | 1.00 | > 98 % | Aladdin |
| | Sodium butane sulfonate | $C_4H_9SO_3Na$ | 2.4 | 0.75 | ≥ 99 % | Aladdin |
| | Sodium pentane sulfonate | $C_5H_{11}SO_3Na$ | 0.8 | 0.60 | 98 % | Aladdin |
| | Sodium heptane sulfonate | $C_7H_{15}SO_3Na$ | 0.6 | 0.43 | 98 % | Macklin |
| | Sodium octane sulfonate | $C_8H_{17}SO_3Na$ | 0.07 | 0.38 | ≥ 99 % | Macklin |
| Organic sulfate | Sodium methyl sulfate | $CH_3SO_4Na$ | 2.6 | 4.00 | 98 % | Energy Chemical |
| | Sodium ethyl sulfate | $C_2H_5SO_4Na$ | 1.5 | 2.00 | 98 % | Meryer |
| | Sodium octyl sulfate | $C_8H_{17}SO_4Na$ | 0.2 | 0.50 | 99 % | Rhawn |
| Dicarboxylic acid | Pimelic acid (PA) | $C_7H_{12}O_4$ | 0.3 | 0.57 | 99 % | Macklin |
| | Phenylmalonic acid (PhMA) | $C_9H_8O_4$ | 0.2 | 0.44 | 98 % | Aladdin |

* For more information, see https://comptox.epa.gov/ (last access: 19 June 2023).

## 2 Materials and methods

### 2.1 Chemicals

NaCl and AS were purchased from Sinopharm Chemical Reagent Co., Ltd (purity ≥ 99.8 %) and Sigma-Aldrich (purity ≥ 99 %), respectively. The studied organic substances include 10 surface active organics (five organosulfonates, three organosulfates, and two dicarboxylic acids). The five organic sulfonates were sodium propane sulfonate ($C_3H_7SO_3Na$), sodium butane sulfonate ($C_4H_9SO_3Na$), sodium pentane sulfonate ($C_5H_{11}SO_3Na$), sodium heptane sulfonate ($C_7H_{15}SO_3Na$), sodium octane sulfonate ($C_8H_{17}SO_3Na$). The three organic sulfates were sodium methyl sulfate ($CH_3SO_4Na$), sodium ethyl sulfate ($C_2H_5SO_4Na$), and sodium octyl sulfate ($C_8H_{17}SO_4Na$). Two dicarboxylic acids were pimelic acid (PA) and phenylmalonic acid (PhMA). Relevant properties of used chemicals were summarized in Table 1. These organic surfactants were of various solubilities, from sparingly soluble (e.g., $0.07\,mol\,L^{-1}$ for $C_8H_{17}SO_4Na$) to highly soluble (e.g., $2.6\,mol\,L^{-1}$ for $CH_3SO_4Na$). O : C ratios were from 0.38 to 4, covering most of the molar ratios in the atmosphere (0.1–1.0; You et al., 2013). The studied organic substances contain functional groups such as sulfonates, sulfates, carboxylic acids, and aromatics, which were universally detected in atmospheric aerosol samples (Takahama et al., 2007).

### 2.2 Aerosol generation and collection

The process of aerosol generation and collection was described in detail by Xiong et al. (2022). In brief, particles were nebulized from solutions of organic and inorganic matter ($\sim 5\,g\,L^{-1}$) mixed with deionized water (Millipore; resistivity = 18.2 MΩ). After drying (RH < 15 %) by a silica gel diffusion dryer, the particles were deposited with an eight-stage non-viable particle sizing sampler (model BGI 20800 series; BGI Incorporated) onto 400 mesh copper grids coated with a carbon film (Zhongjingkeyi Films Technology Co. Ltd). Copper grids were mounted on the seventh stage, selecting particles with an aerodynamic size of 0.7–1 µm. Collected samples were stored under dry conditions (RH < 10 %) and were immediately characterized within 24 h to avoid possible sample aging.

### 2.3 Mixing state observation

Optical microscopy (Ciobanu et al., 2009; Bertram et al., 2011; Song et al., 2012a, b; You et al., 2013), a microfluidic device (Roy et al., 2020), cryo-TEM (Veghte et al., 2014; Freedman, 2020; Ott and Freedman, 2021; Ott et al., 2021; Zhang et al., 2022), ESEM (O'Brien et al., 2015), optical tweezers (Stewart et al., 2015; Tong et al., 2022), and an F-AFT (fluorescence aerosol flow tube; Ohno et al., 2021, 2023) were the methods reported in the literature for detecting the aerosol mixing state. Optical microscopy and the microfluidic device were the commonly used direct methods for substrate-supported droplets but were limited by the size range (at least dozens of micrometers). Optical tweezers and F-AFT could investigate LLPS in a levitated micrometer and submicrometer droplet, respectively, but these are indirect ways, although there are no distinct differences in SRH results when comparing them to substrate-supported droplets (Ohno et al., 2023). Cryo-TEM and ESEM could detect the mixing state at a submicrometer scale, but damage caused by the electron beam may exist (depending on the chemistry and

beam parameter settings). Ott et al. (2021) give some useful suggestions for minimizing the damage, e.g., decreasing the exposure time and the amount of electron dosage.

The mixing state was observed by using environmental scanning electron microscopy (ESEM; Thermo Scientific Quattro S) with a temperature-controlled stage. The temperature in the chamber varied between 0.1 and ∼ 25 °C, and the RH in the chamber was controlled by adjusting the temperature (±0.1 °C) at a predefined pressure (610 Pa). In each experiment, particles with lateral dimensions of ∼ 1 µm were selected first (based on the deposition, the volume-equivalent size was smaller than 1 µm). Then the RH was raised from a low (∼ 30 %) to a high condition (∼ 100 %) at the change rate of 2 %–3 % RH per minute. High RH lasted for at least 5 min for equilibrium, promising complete dissolution of solutes (O'Brien et al., 2015). With increased RH, most selected particles grew larger (several micrometers in size) before the subsequent LLPS experiment. Then, the RH decreased to a dry condition at similar change rate. A negligible influence on the LLPS of the AS–organic (O'Brien et al., 2015; You and Bertram, 2015) and NaCl–organic systems (Roy et al., 2020) in the micrometer scale (from several micrometers to dozens of micrometers) was observed. Cloud parcel modeling suggests that atmospheric RH fluctuations typically occur from 0 % $min^{-1}$ to 3.6 % $min^{-1}$ (Pöhlker et al., 2014). Therefore, we assume that the water uptake in our experiments approximates the atmospheric conditions (Shiraiwa et al., 2013). Images of mixing states during the whole RH period were acquired at an electron acceleration voltage of 30 kV. The detector used for the ESEM imaging was a scanning transmission electron detector. The images were recorded with line scanning rates of 3–5 µs to minimize the possible beam damage (see the supplement of O'Brien et al., 2015). The varying range of the RH values between two consecutive pictures was mostly 0.2 %–0.4 % RH (very narrow), which was necessary in order to capture the possible quick transitions of the mixing states. Each image in our study contained at least five particles (or droplets) to ensure the reproducibility of the ESEM and also to decrease the uncertainty. In addition, we have repeated some parts of the experiment (e.g., in the RH decreasing period) to validate the reproducibility, and the results showed a good agreement (Fig. S1 in the Supplement).

## 3 Results and discussion

### 3.1 Mixing states upon hydration

Deliquescence RH (DRH) and efflorescence RH (ERH) of pure NaCl (Figs. 1a–d and S2a–b) and AS particles (Figs. 2a–d and S2c–d) were firstly tested via the experimental setup. The DRH of NaCl and AS was observed at 80.9 ± 0.1 % (literature values of 77 ± 1 %; Pöhlker et al., 2014) and 82.1 ± 0.6 % (literature values of 82.0 %; Onasch et al., 1999). The ERH of NaCl and AS was 48.3 ± 0.4 % (literature values of 48 ± 2 %; Zeng et al., 2014) and 30.7 ± 0.9 % (literature values of 31 ± 1 %; Cheng and Kuwata, 2023). Generally, the experimental DRH and ERH values correspond well with those in the literature, confirming the reliability of the experimental setup. The DRH of the NaCl showed a slight deviation by about nearly 4 %, which could be explained by kinetic effects, which is when the system had not reached full equilibrium (Pöhlker et al., 2014). Before deliquescence, the substrate-supported NaCl and AS particles both showed substantial water uptake, thus forming an aqueous halo around a solid core. Similar observational results of NaCl and AS have been reported and could be explained by interactions at the sample–substrate interface, which plays an important role in such a gradual phase transition as an additional energy term (Wise et al., 2008; Pöhlker et al., 2014).

Figures 1e and 2e illustrate the two separated phases with a dark core (blue arrow) and bright shell (green arrow) of dry deposited NaCl–$C_2H_5SO_4Na$ and AS–$C_2H_5SO_4Na$ particles. The dark cores are indicated as being inorganics because darker regions are characteristic of areas with higher atomic number elements (e.g., Cl) and/or a thicker sample region (Laskin et al., 2006; O'Brien et al., 2015). Phase separations with a core shell structure were observed for all studied inorganic salt–organic surfactant systems. This may be attributed to the size range of the particles we investigated (∼ 1 µm with dry lateral dimension), since inorganic salt–organic surfactant particles with such a size range might overcome the energy barrier needed to form a new phase (Altaf and Freedman, 2017; Altaf et al., 2018; Freedman, 2020; Ott and Freedman, 2021). According to the results in Freedman (2020), the morphology of most systems was found to be dependent on size, where large particles were phase-separated and small particles were homogeneous. Furthermore, all systems (e.g., AS–PA and AS–succinic acid systems) with dry diameters larger than 0.7 µm were observed as being phase-separated regardless of the occurrence of size dependence (Altaf and Freedman, 2017). Freedman (2020) expected that the phase separation could be attributed to the nucleation and growth; therefore, larger particles tended to have a phase-separated morphology. In another study, Ohno et al. (2021) also found that LLPS occurred at lower RH in smaller droplets (70–190 nm) than in larger droplets (260–370 nm).

When the RH increased from a dry level, as the organic phase slowly absorbed water, the NaCl and AS cores were not fully dissolved at RH levels of between 90.1 % and 91.7 % (Figs. 1g and 2g), respectively, and were notably higher than the DRH. The phenomenon was found for all NaCl–organic surfactant systems and AS–organic surfactant systems, and the DRH of the inorganic salts ranged from 88.3 % to 99.5 % (Figs. 1i and 2i). Laskina et al. (2015) measured the DRH of pure AS and NaCl at submicrometer (100 nm) and supermicrometer (3–10 µm) size ranges with hygroscopic tandem differential mobility analyzers (HTDMAs) and micro Raman spectroscopy, respectively, and the

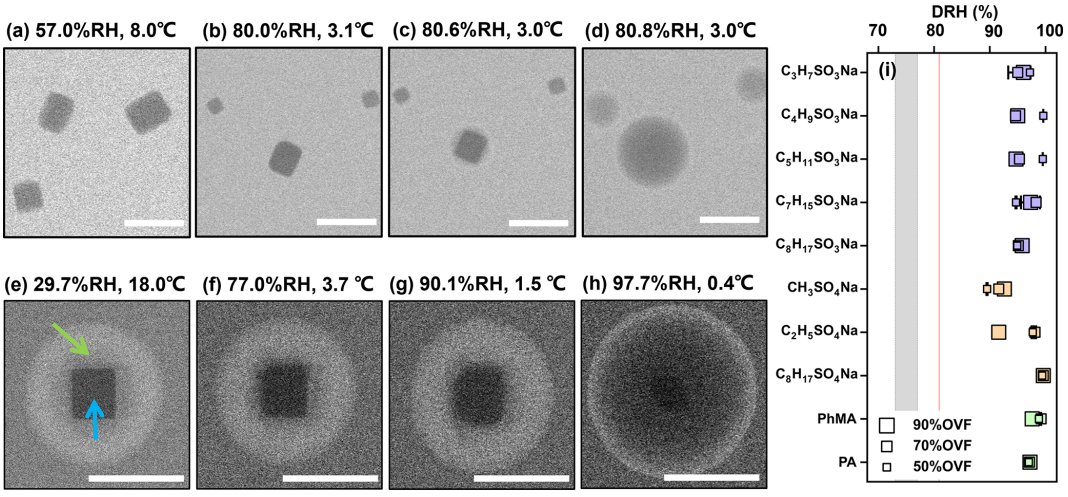


**Figure 1.** ESEM images of **(a–d)** pure NaCl and **(e–h)** NaCl–$C_2H_5SO_4Na$ (70 % OVF) with different RH. Blue and green arrows indicate the inorganic phase and organic phase, respectively. The RH value shows that the NaCl core fully dissolved (DRH) for NaCl–organic surfactant systems with different OVF **(i)**. The gray area in panel **(i)** covers the DRH range of NaCl in the literature (obtained from Peng et al., 2022). The red line indicates the measured average DRH of pure NaCl (80.9 ± 0.1 %). Scale bars in panels **(a)**–**(h)** were 1 µm.

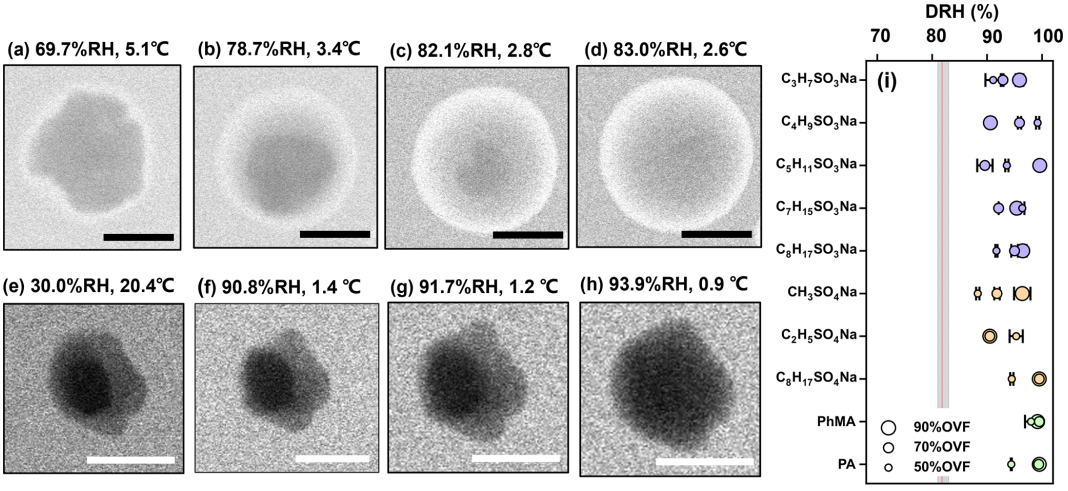


**Figure 2.** ESEM images of **(a–d)** pure AS and **(e–h)** AS–$C_2H_5SO_4Na$ (50 % OVF) with different RH. Blue and green arrows indicate the inorganic phase and organic phase, respectively. The RH value shows that the AS core fully dissolved (DRH) for AS–organic surfactant systems with different OVF **(i)**. The gray area in panel **(i)** covers the DRH range of AS in the literature (obtained from Peng et al., 2022). The red line indicates the measured average DRH of pure AS (82.1 ± 0.6 %). Scale bars in panels **(a)**–**(h)** were 1 µm.

deviations between them were both within 3 %, indicating that the DRH of pure AS and NaCl showed weak size dependence (> 100 nm). In addition, Cheng and Kuwata (2023) used a low-temperature hygroscopicity tandem differential mobility analyzer (low-T HTDMA) and observed a consistent DRH of NaCl and AS within experimental error under temperatures ranging from −10 to 22.5 °C, suggesting that the DRH of NaCl and AS experience no temperature dependence. According to the abovementioned studies, a DRH of pure AS and NaCl displayed a weak dependence on size (> 100 nm) and temperature, and we therefore concluded that the surfactant shell inhibits the water diffusion exposing it to inorganic cores, thus resulting in delays of the deliquescence of inorganic cores. The inhibition of the surfactant shell could be triggered by increased viscosity with raised RH, since reported studies have reported that organic shells can transform from solid to semisolid states with high viscosity under wet conditions (Zhang et al., 2018). In a RH-constrained lab study at constant room temperature, Li et al. (2021) also observed that the organic coating of secondary organic aerosol (oxidizing $\alpha$-pinene) started to deliquesce first, but the phase changes in the AS cores from solid to liquid took place at 83 %–90 % RH, which is lower than those in the current study. This was possibly caused by the water dif-

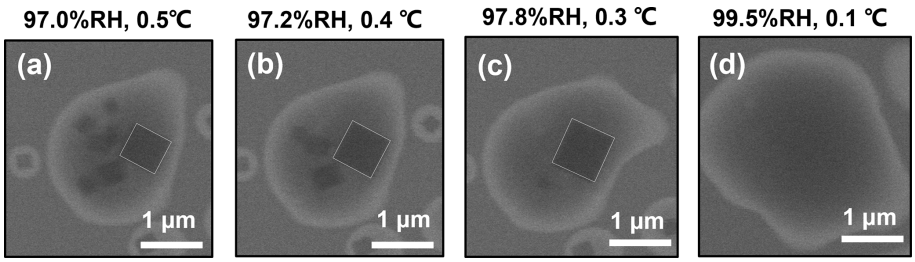


**Figure 3.** ESEM images of Ostwald ripening for NaCl–$C_8H_{17}SO_4Na$ (50 % OVF) particles. The white square indicates the biggest NaCl core (assumed square) in the droplet. The biggest NaCl grew larger (recrystallization), while the small NaCl cores dissolved.

fusion coefficient through the organic phase, which could be affected by organic species and environment parameters such as temperature. As given by Nguyen et al. (2017), the diffusion coefficient of a water molecule through an organic shell could be decreased by a lower temperature. In the current study, a higher RH in the ESEM chamber was achieved by decreasing the temperature; thus, this might decrease the diffusion coefficient of water in an organic surfactant and lead to higher DRH than that in Li et al. (2021). In previous studies and the current work, it was indicated that the phenomenon (water inhibition by organic coating) is a common and important procedure that affects ambient aerosol hygroscopicity because inorganic–organic core shell structures were ubiquitously observed in the field (Li et al., 2016, 2021; Unga et al., 2018; Xu et al., 2020; Wang et al., 2021; Zhang et al., 2022). Though the water inhibition of an organic shell in the current study was observed at temperature much lower than room temperature, it is meaningful and may affect the aerosol properties in some special area, such as polar regions (Lambert et al., 2013; Kirpes et al., 2022; Závacká et al., 2022) or winter time periods (Xu et al., 2021; Zhang et al., 2021) that are characteristic of low-temperature environments.

A previous study believed that deliquescence in the hydration of inorganics took place independently of the circumstances. However, Fig. 3 illustrates an unexpected phase transition of NaCl cores coated with $C_2H_5SO_4Na$. As shown in Fig. 3a, a droplet with several NaCl cores was observed at 97.0 % RH, since, as discussed above, the organic shell inhibits water diffusion. The NaCl cores in the droplet were bigger ones (marked by white squares), and the rest were smaller. When the RH gradually raised (Fig. 3b and c) as smaller NaCl cores serially deliquesced and dissolved, the size of the bigger NaCl core surprisingly increased, indicating a simultaneous NaCl recrystallization at the expense of smaller ones (i.e., Ostwald ripening; Boistelle and Astier, 1988). After other small particles totally dissolved, the bigger NaCl core deliquesced and fully dissolved at 99.5 % RH (Fig. 3d). A previous study reported on the "efflorescence upon hydration" for 1 : 1 mixed NaCl–gluconic acid and AS–gluconic acid with optical tweezers (Zhu et al., 2022). Based on the infrared (IR) spectrum, they found the coexistence of a partial efflorescence mixed state, ultraviscous state, and liquid state during the "efflorescence upon hydration" period, indicating an unstable crystal and concentrated liquid state of NaCl. Under these circumstances, Ostwald ripening can take place. Ostwald ripening was triggered by the decrease in total system's free energy, since dissolved small and effloresced large crystals reduce the total system's free energy (Voorhees, 1985). We directly observed obvious Ostwald ripening processes in 6 out of the 10 NaCl–organic surfactant systems. As a result of the water inhibition by the surfactant shell discussed above, here Ostwald ripening occurred at RH levels above 90 %, which were notably higher than the reported 75 %–77 % for pure NaCl measured by X-ray microspectroscopy at 27 °C (Pöhlker et al., 2014).

## 3.2 Mixing states upon dehydration

### 3.2.1 LLPS

In Fig. 4a, AS–$C_8H_{17}SO_4Na$ was homogeneous under RH of 99.5 %. When RH decreased to 99.1%, the particles showed two separated liquid phases (i.e., LLPS), with a dark inner phase and a light outer phase (Fig. 4b), which are highlighted by the blue and green arrows. In addition, the AS–$C_8H_{17}SO_4Na$ remained in a LLPS state when RH continued to decline until the efflorescence of the inner inorganic phase occurred (Fig. 4c). In our study, 8 out of 20 chemical systems underwent LLPS, including four AS–organic surfactant systems and four NaCl–organic surfactant systems. Figure 5 illustrates the relationship between LLPS occurrence and the molar ratios (O : C and H : C) of the surface-active organics as per the reported results of other binary inorganic salt–organic systems in the literature (Bertram et al., 2011; You et al., 2013; You and Bertram, 2015). In our study, LLPS always occurs when the O : C ratio is below 0.43 (dashed yellow line in Fig. 5) for NaCl–organic surfactant and AS–organic surfactant droplets. This value was close to the reported values in You et al. (2013; $\sim$ 0.5). However, in their results, LLPS was never observed when O : C was above $\sim$ 0.8 (dashed gray line in Fig. 5; Bertram et al., 2011; Song et al., 2012b; You et al., 2013), which was higher than that in our experiment (0.57). We ascribe this to the insufficient chemical systems in our experiment (10 systems), which were notably smaller than in previous studies (over 30). As a result,

the bounds of O : C determining LLPS were not changed if our results were added to previous studies such as You et al. (2013) and Song et al. (2012b).

In order to analyze the effect of inorganic salts in LLPS, we compared the SRH of systems which contained the same organic matter but different inorganic salts. Results showed that the SRH values of AS–$C_8H_{17}SO_4Na$ (70 % OVF), AS–$C_8H_{17}SO_3Na$ (90 % OVF), AS–PhMA (90 % OVF), and AS–PA (90 % OVF) were 98.7 ± 0.5 %, 81.3 ± 1.2 %, 97.9 ± 1.0 %, and 98.5 ± 0.8 % and were all notably higher than the SRH of the corresponding NaCl-containing systems (92.5 ± 3.9 %, 56.4 ± 1.2 %, 85.6 ± 3.6 %, and 66.7 ± 0.8 %), respectively. This was attributed to the different salting-out efficiency of inorganic salts, since You et al. (2013) found that the SRH of inorganic–organic mixtures followed the trend of $(NH_4)_2SO_4 \geq NH_4HSO_4 \geq NaCl \geq NH_4NO_3$, which was generally consistent with the salting-out efficiency.

The measured SRH values as a function of OVF are plotted in Fig. 6. AS–$C_8H_{17}SO_4Na$ showed a SRH of 98.7 ± 0.5 % when OVF was 70 %, which is higher than those of 50 % OVF (82.1 ± 1.6 %) and 90 % OVF (80.0 ± 0.9 %). However, the phenomenon was totally different from that of AS–$C_8H_{17}SO_3Na$, which showed lower SRH with 70 % OVF (62.2 ± 2.6 %), compared to those of 50 % OVF (69.6 ± 1.0 %) and 90 % OVF (81.3 ± 1.2 %). Therefore, the above results indicate the controversial effect of OVF on SRH (Bertram et al., 2011; Song et al., 2012a).

### 3.2.2 Solid-phase separation

For mixed systems that do not undergo LLPS, we found that they were separated with distinct core shell phases from a homogeneous morphology at low RH. However, this phase transition was different from LLPS, since the inner phase was with an irregular shape (LLPS occurred with a rounded inner liquid phase), which was attributed to the efflorescence progress of the inorganic salt (Fig. 7). Therefore, we termed it a solid-phase separation. The efflorescence RH (ERH) of the inner inorganic salt, therefore, was the solid-phase separation RH.

In Fig. 8a, the ERH of NaCl–organic surfactant particles with 50 %, 70 %, and 90 % OVF ranged between 47.0 % and 61.8 %, which was higher than the measured ERH (48.3 ± 0.4 %) and reported ERH range of pure NaCl (41 %–51 %; Peng et al., 2022). This could be explained by the interaction between organic and inorganic matter. For example, Ghorai et al. (2014) found an acid displacement reaction in NaCl–glutaric acid systems, which was driven by gaseous HCl liberation and caused chloride depletion. Such interactions of chloride depletion may facilitate the efflorescence transitions, resulting in efflorescence at ∼ 68 % RH and ∼ 60 % RH, respectively, for internally mixed NaCl–glutaric acid particles with molar ratios of 1 : 3 and 1 : 1. Higher ERH could also be attributed to heterogeneous nucleation initiated by chemical purities (Choi and Chan, 2002). Choi and Chan (2002) observed 54.4 % ERH for a 1 : 1 mixed NaCl–glutaric acid, and they explained that insoluble additives crystallized and formed nuclei for the heterogeneous efflorescence of inorganic salts, leading to their higher ERH values.

As for AS–organic surfactant systems (Fig. 8b), efflorescence was observed for 27 out of 30 aerosol samples. We did not observe a distinct occurrence of efflorescence for the remaining three samples, and two samples out of three had 90 % OVF, which could be explained by the possible loss of AS when it is persistently exposed to an electronic beam (Posfai et al., 2013; O'Brien et al., 2015), especially for particles in which inorganic fractions were small (i.e., high OVF). ERH values of AS–organic surfactant particles with 50 %, 70 %, and 90 % OVF ranged from 31.2 % to 46.6 %, showing a close agreement to the reported ERH of pure AS (30 %–48 %; Peng et al., 2022), but the result was higher than the measured ERH (30.7 ± 0.9 %). The potential cause may be the heterogeneous crystallization of AS on organic salts (Wang et al., 2019; Yang et al., 2019; Ma et al., 2021). For example, Wang et al. (2019) investigated the efflorescence of AS in AS–sodium oxalate and found that SRH values were between 48.9 % and 55.3 % with organic–inorganic mole ratios of 1 : 1 and 3 : 1, respectively, which were higher than that of pure AS (47.5 %). It is likely, as Yang et al. (2019) also observed, that the initial ERH of AS rose to between 47.7 % and 62 % for inorganic mole ratios of 1 : 3 and 1 : 1 AS–sodium pyruvate mixtures, respectively.

## 3.3 Atmospheric implication

Dicarboxylic acids, organosulfates, and organosulfonates are important surface-active organic constituents in secondary organic aerosol. Few studies comprehensively studied their mixing state following fluctuating RH cycling, which is a simulation of real atmospheric conditions. In this work, we concluded that the mixing state affected the interactions of inorganic salt with water. Since common assumptions in chemical transport models (including ISORROPIA II, EQSAM, and MOSAIC; Fountoukis and Nenes, 2007, Metzger et al., 2002a, b, and Zaveri et al., 2008, respectively) are that the water uptake is determined separately by the inorganic compounds and organics (i.e., the effect of mixing state is ignored; Myhre et al., 2007; Nandy et al., 2021), our results implied a further effect of mixing states on the estimations of aerosol hygroscopicity (e.g., growth factor), optical properties, and radiative forcing.

During dehydration, we investigated the phase-separated efflorescence (before and after) for inorganic salt–organic surfactant particles. When compared with homogeneous particles, the phase-separated particles could decrease the trace gas uptake (You et al., 2012), resulting in reduction in the formation of secondary organic aerosols (SOAs; Zhang et al., 2018). In addition, the organic phase was enriched in an "outer shell", which can potentially alter the aerosol water

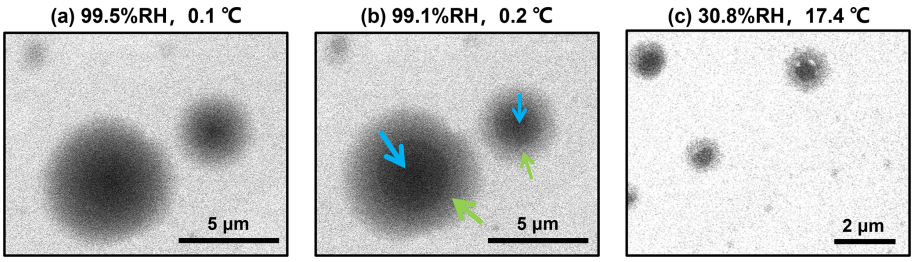


**Figure 4.** ESEM images of **(a)** homogeneous AS–$C_8H_{17}SO_4Na$ particles (70 % OVF) that underwent **(b)** LLPS and **(c)** efflorescence, with a dark inner phase and a light outer phase shown in panel **(b)**, which are highlighted by the blue and green arrows

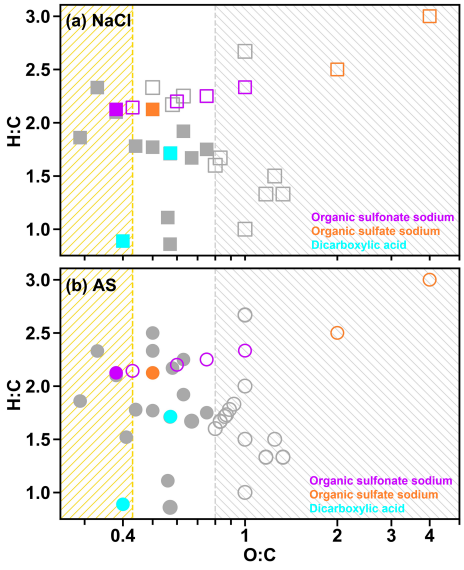


**Figure 5.** Van Krevelen diagram for the mixed inorganic surfactant particles in the current study (symbols shown in red, orange, and cyan). **(a)** NaCl–organic surfactant systems. **(b)** AS–organic surfactant systems. Solid symbols indicate that LLPS was observed for particles with at least one OVF, while hollow symbols indicate that LLPS was not observed for particles with different OVFs. Symbols in gray in panels **(a)** and **(b)** were the results obtained from Bertram et al. (2011), You et al. (2013), and You and Bertram (2015). The yellow hatched region ($O:C < 0.43$) means that LLPS was observed in all investigated systems, while the gray hatched region ($O:C > 0.8$) means that no LLPS was detected in any of the investigated systems.

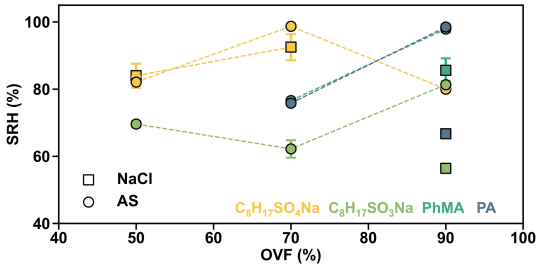


**Figure 6.** Summary of the SRH results as a function of OVF for inorganic surfactant particles.

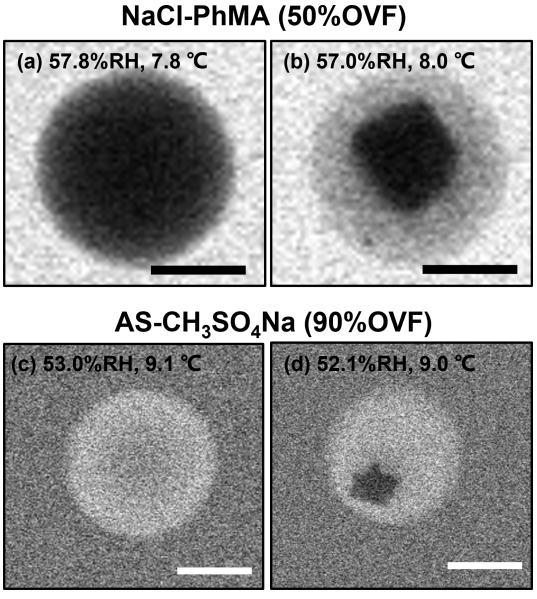


**Figure 7.** ESEM images of solid-phase separation for **(a, b)** NaCl–PhMA and **(c, d)** AS–$CH_3SO_4Na$ systems. The scale bars in **(a)**–**(d)** were 500 nm.

activity and lower the aerosol surface tension, hence affecting aerosol–cloud interactions because the water uptake of organic matter in current models (e.g., MPMPO and SOA treatment in CMAQ v5.2; Griffin et al., 2003, and Pye et al., 2017, respectively) is estimated by highly parameterized relationships that assume ideal solutions, using the kappa hygroscopicity parameter with water surface tension (Petters and Kreidenweis, 2007; Nandy et al., 2021).

Our results provide comprehensive information on mixing states between inorganic salts and organic surfactant from a nanoscale perspective, which could help establish the incorporation of atmospheric modeling to improve predictions on the indirect effects of aerosol–climate interactions. We should note that in the atmosphere, most particles are smaller (e.g., 0.1 to 0.3 μm) than the sample particles, and the chemical characteristics of ambient aerosol are not as simple as the binary chemical systems in the current study. Therefore,

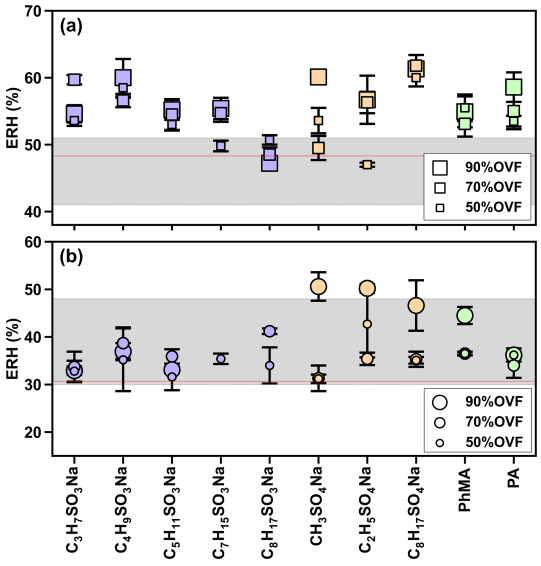


**Figure 8.** Measurements of the efflorescence relative humidity (ERH) of **(a)** NaCl–organic surfactant and **(b)** AS–organic surfactant particles. The gray areas in panels **(a)** and **(b)** indicate the efflorescence RH range of NaCl (41 %–51 %) and AS (30 %–48 %), as obtained from Peng et al. (2022). Red lines in panels **(a)** and **(b)** represent the measured average ERH of pure NaCl ($48.3 \pm 0.4$ %) and AS ($30.7 \pm 0.9$ %).

in the future, the water kinetic inhibition should be further investigated for smaller particles containing more complex systems.

## 4 Conclusions

Atmospheric surfactants have the potential to be distributed to the surface, altering the mixing state and influencing aerosol hygroscopicity and CCN activity. Currently, direct observations of the RH-dependent mixing state of aerosol containing atmospheric surfactants is scarce. In this study, dynamic mixing states and phase transitions of 20 types of submicron particles containing inorganic and surface-active organic constituents were directly investigated upon relative humidity (RH) cycling by environmental scanning electron microscopy (ESEM).

Inorganic–organic core shell morphology was found for dry deposited mixed inorganic salt–organic surfactant particles. During hydration, the organic shell inhibited water diffusion to the inorganic cores, resulting in the higher-deliquescence RH (88.3 %–99.5 %) of the inner inorganic phase when compared with pure inorganic aerosol. This was because higher RH levels may facilitate the phase transition of an organic shell from solid to semisolid, thereby raising the organic viscosity and decreasing water diffusion leading to the exposure of the inorganic core. Meanwhile, we directly observed an obvious Ostwald ripening of NaCl (that is, the growth of larger NaCl crystals at the expense of smaller ones) in 6 out of 10 NaCl–organic surfactant systems. As a result of the water inhibition by the surfactant shell, Ostwald ripening in all systems occurred at RH levels above 90 %, which were higher than reported RH range of pure NaCl measured at 27 °C (75 %–77 %).

During dehydration, 8 out of 20 chemical systems underwent LLPS, including four AS–organic surfactant systems and four NaCl–organic surfactant systems. LLPS was always observed when $O:C \leq 0.4$ and never observed when $O:C > \sim 0.57$. SRH values of AS–organic surfactant particles were generally higher than SRH of corresponding NaCl–organic surfactant systems, which was consistent with the reported salting-out efficiency of inorganic salts. OVF showed a controversial effect on the SRH of inorganic salt–organic surfactant systems. Additionally, inorganic salt–organic surfactant systems without LLPS underwent solid-phase separation after efflorescence and also showed distinctly separated phases. Our results provide comprehensive and unique insights into the dynamic evolution of inorganic salt–organic surfactant particles under fluctuating atmospheric conditions, which could help improve our fundamental knowledge and decrease the uncertainty in the model estimation with regard to the global radiative effect.

**Data availability.** The experimental data are available via Zenodo (https://doi.org/10.5281/zenodo.8079001, Xiong et al., 2023).

**Supplement.** The supplement related to this article is available online at: https://doi.org/10.5194/acp-23-8979-2023-supplement.

**Author contributions.** CX and BK did the experiments and analyzed the data. CX plotted the figures and wrote the original draft. FZ and XP contributed to the discussion and reviewed the paper. BK and ZX reviewed the paper and contributed to the funding acquisition. ZW administrated the project, conceptualized the study, reviewed the paper, and contributed to the funding acquisition.

**Competing interests.** At least one of the (co-)authors is a member of the editorial board of *Atmospheric Chemistry and Physics*. The peer-review process was guided by an independent editor, and the authors also have no other competing interests to declare.

**Disclaimer.** Publisher's note: Copernicus Publications remains neutral with regard to jurisdictional claims in published maps and institutional affiliations.

**Acknowledgements.** We thank Yuzhong Zhang from the School of Engineering at Westlake University and Lin Liu and Wenjing Cao from the Instrumentation and Service Center for Physical Sciences

at Westlake University for the supporting in environmental scanning electron microscopy experiments.

**Financial support.** This research has been supported by the National Natural Science Foundation of China (grant nos. 91844301, 41805100, 42005087, and 42005086) and the Key Research and Development Program of Zhejiang Province (grant nos. 2021C03165 and 2022C03084).

**Review statement.** This paper was edited by Allan Bertram and reviewed by two anonymous referees.

## References

Altaf, M. B. and Freedman, M. A.: Effect of Drying Rate on Aerosol Particle Morphology, J. Phys. Chem. Lett., 8, 3613–3618, https://doi.org/10.1021/acs.jpclett.7b01327, 2017.

Altaf, M. B., Dutcher, D. D., Raymond, T. M., and Freedman, M. A.: Effect of Particle Morphology on Cloud Condensation Nuclei Activity, ACS Earth Space Chem., 2, 634–639, https://doi.org/10.1021/acsearthspacechem.7b00146, 2018.

Bertram, A. K., Martin, S. T., Hanna, S. J., Smith, M. L., Bodsworth, A., Chen, Q., Kuwata, M., Liu, A., You, Y., and Zorn, S. R.: Predicting the Relative Humidities of Liquid-Liquid Phase Separation, Efflorescence, and Deliquescence of Mixed Particles of Ammonium Sulfate, Organic Material, and Water Using the Organic-to-Sulfate Mass Ratio of the Particle and the Oxygen-to-Carbon Elemental Ratio of the Organic Component, Atmos. Chem. Phys., 11, 10995–11006, https://doi.org/10.5194/acp-11-10995-2011, 2011.

Boistelle, R. and Astier, J. P.: Crystallization Mechanisms in Solution, J. Cryst. Growth, 90, 14–30, https://doi.org/10.1016/0022-0248(88)90294-1, 1988.

Bruggemann, M., Xu, R. S., Tilgner, A., Kwong, K. C., Mutzel, A., Poon, H. Y., Otto, T., Schaefer, T., Poulain, L., Chan, M. N., and Herrmann, H.: Organosulfates in Ambient Aerosol: State of Knowledge and Future Research Directions on Formation, Abundance, Fate, and Importance, Environ. Sci. Technol., 54, 3767–3782, https://doi.org/10.1021/acs.est.9b06751, 2020.

Cheng, M. Q. and Kuwata, M.: Development of the Low-Temperature Hygroscopicity Tandem Differential Mobility Analyzer (Low-T HTDMA) and its Application to $(NH_4)_2SO_4$ and NaCl Particles, J. Aerosol Sci., 168, 106111, https://doi.org/10.1016/j.jaerosci.2022.106111, 2023.

Choi, M. Y. and Chan, C. K.: The Effects of Organic Species on the Hygroscopic Behaviors of Inorganic Aerosols, Environ. Sci. Technol., 36, 2422–2428, https://doi.org/10.1021/es0113293, 2002.

Ciobanu, V. G., Marcolli, C., Krieger, U. K., Weers, U., and Peter, T.: Liquid-Liquid Phase Separation in Mixed Organic/Inorganic Aerosol Particles, J. Phys. Chem. A, 113, 10966–10978, https://doi.org/10.1021/jp905054d, 2009.

Fountoukis, C. and Nenes, A.: ISORROPIA II: a computationally efficient thermodynamic equilibrium model for $K^+$–$Ca_2^+$–$Mg_2^+$–$NH_4^+$–$Na^+$–$SO_4^{2-}$–$NO_3$–Cl–$H_2O$ aerosols, Atmos. Chem. Phys., 7, 4639–4659, https://doi.org/10.5194/acp-7-4639-2007, 2007.

Freedman, M. A.: Liquid-Liquid Phase Separation in Supermicrometer and Submicrometer Aerosol Particles, Acc. Chem. Res., 53, 1102–1110, https://doi.org/10.1021/acs.accounts.0c00093, 2020.

Ghorai, S., Wang, B. B., Tivanski, A., and Laskin, A.: Hygroscopic Properties of Internally Mixed Particles Composed of NaCl and Water-Soluble Organic Acids, Environ. Sci. Technol., 48, 2234–2241, https://doi.org/10.1021/es404727u, 2014.

Griffin, R. J., Nguyen, K., Dabdub, D., and Seinfeld, J. H.: A coupled hydrophobic-hydrophilic model for predicting secondary organic aerosol formation, J. Atmos. Chem., 44, 171–190, https://doi.org/10.1023/A:1022436813699, 2003.

Guo, L. Y., Peng, C., Zong, T. M., Gu, W. J., Ma, Q. X., Wu, Z. J., Wang, Z., Ding, X., Hu, M., Wang, X. M., and Tang, M. J.: Comprehensive Characterization of Hygroscopic Properties of Methanesulfonates, Atmos. Environ., 224, 117349, https://doi.org/10.1016/j.atmosenv.2020.117349, 2020.

Ho, K. F., Lee, S. C., Ho, S. S. H., Kawamura, K., Tachibana, E., Cheng, Y., and Zhu, T.: Dicarboxylic acids, ketocarboxylic acids, $\alpha$-dicarbonyls, fatty acids, and benzoic acid in urban aerosols collected during the 2006 Campaign of Air Quality Research in Beijing (CAREBeijing-2006), J. Geophys. Res.-Atmos., 115, D19312, https://doi.org/10.1029/2009jd013304, 2010.

Hyder, M., Genberg, J., Sandahl, M., Swietlicki, E., and Jönsson, J. Å.: Yearly trend of dicarboxylic acids in organic aerosols from south of Sweden and source attribution, Atmos. Environ., 57, 197–204, https://doi.org/10.1016/j.atmosenv.2012.04.027, 2012.

Kirpes, R. M., Lei, Z. Y., Fraund, M., Gunsch, M. J., May, N. W., Barrett, T. E., Moffett, C. E., Schauer, A. J., Alexander, B., Upchurch, L. M., China, S., Quinn, P. K., Moffet, R. C., Laskin, A., Sheesley, R. J., Pratt, K. A., and Ault, A. P.: Solid organic-coated ammonium sulfate particles at high relative humidity in the summertime Arctic atmosphere, P. Natl. Acad. Sci. USA, 119, e2104496119, https://doi.org/10.1073/pnas.2104496119, 2022.

Kwamena, N. O. A., Buajarern, J., and Reid, J. P.: Equilibrium Morphology of Mixed Organic/Inorganic/Aqueous Aerosol Droplets: Investigating the Effect of Relative Humidity and Surfactants, J. Phys. Chem. A, 114, 5787–5795, https://doi.org/10.1021/jp1003648, 2010.

Lambert, F., Kug, J. S., Park, R. J., Mahowald, N., Winckler, G., Abe-Ouchi, A., O'Ishi, R., Takemura, T., and Lee, J. H.: The role of mineral-dust aerosols in polar temperature amplification, Nat. Clim. Change, 3, 487–491, https://doi.org/10.1038/Nclimate1785, 2013.

Laskin, A., Cowin, J. P., and Iedema, M. J.: Analysis of Individual Environmental Particles using Modern Methods of Electron Microscopy and X-ray Microanalysis, J. Electron. Spectrosc. Relat. Phenom., 150, 260–274, https://doi.org/10.1016/j.elspec.2005.06.008, 2006.

Laskina, O., Morris, H. S., Grandquist, J. R., Qiu, Z., Stone, E. A., Tivanski, A. V., and Grassian, V. H.: Size Matters in the Water Uptake and Hygroscopic Growth of Atmospherically Relevant Multicomponent Aerosol Particles, J. Phys. Chem. A, 119, 4489–4497, https://doi.org/10.1021/jp510268p, 2015.

Li, W. J., Shao, L. Y., Zhang, D. Z., Ro, C. U., Hu, M., Bi, X. H., Geng, H., Matsuki, A., Niu, H. Y., and Chen, J. M.: A review of single aerosol particle studies in the atmosphere of East Asia: morphology, mixing state, source, and

heterogeneous reactions, J. Clean. Product., 112, 1330–1349, https://doi.org/10.1016/j.jclepro.2015.04.050, 2016.

Li, W. J., Teng, X. M., Chen, X. Y., Liu, L., Xu, L., Zhang, J., Wang, Y. Y., Zhang, Y., and Shi, Z. B.: Organic Coating Reduces Hygroscopic Growth of Phase-Separated Aerosol Particles, Environ. Sci. Technol., 55, 16339–16346, https://doi.org/10.1021/acs.est.1c05901, 2021.

Ma, S. S., Pang, S. F., Li, J., and Zhang, Y. H.: A review of efflorescence kinetics studies on atmospherically relevant particles, Chemosphere, 277, 130320, https://doi.org/10.1016/j.chemosphere.2021.130320, 2021.

Martin, S. T.: Phase Transitions of Aqueous Atmospheric Particles, Chem. Rev., 100, 3403–3453, https://doi.org/10.1021/cr990034t, 2000.

Metzger, S., Dentener, F., Krol, M., Jeuken, A., and Lelieveld, J.: Gas/aerosol partitioning 2. Global modeling results, J. Geophys. Res.-Atmos., 107, ACH 17-1–ACH 17-23, https://doi.org/10.1029/2001jd001103, 2002a.

Metzger, S., Dentener, F., Pandis, S., and Lelieveld, J.: Gas/aerosol partitioning 1. A computationally efficient model, J. Geophys. Res.-Atmos., 107, 4312, https://doi.org/10.1029/2001jd001102, 2002b.

Myhre, G., Bellouin, N., Berglen, T. F., Berntsen, T. K., Boucher, O., Grini, A., Isaksen, I. S. A., Johnsrud, M., Mishchenko, M. I., Stordal, F., and Tanre, D.: Comparison of the radiative properties and direct radiative effect of aerosols from a global aerosol model and remote sensing data over ocean, Tellus B, 59, 115–129, https://doi.org/10.1111/j.1600-0889.2006.00238.x, 2007.

Nandy, L., Yao, Y., Zheng, Z. H., and Riemer, N.: Water uptake and optical properties of mixed organic-inorganic particles, Aerosol Sci. Tech., 55, 1398–1413, https://doi.org/10.1080/02786826.2021.1966378, 2021.

Nguyen, Q. T., Kjær, K. H., Kling, K. I., Boesen, T., and Bilde, M.: Impact of Fatty Acid Coating on the CCN Activity of Sea Salt Particles, Tellus B, 69, 1304064, https://doi.org/10.1080/16000889.2017.1304064, 2017.

Noziere, B.: Don't Forget the Surface, Science, 351, 1396–1397, https://doi.org/10.1126/science.aaf3253, 2016.

O'Brien, R. E., Wang, B. B., Kelly, S. T., Lundt, N., You, Y., Bertram, A. K., Leone, S. R., Laskin, A., and Gilles, M. K.: Liquid-Liquid Phase Separation in Aerosol Particles: Imaging at the Nanometer Scale, Environ. Sci. Technol., 49, 4995–5002, https://doi.org/10.1021/acs.est.5b00062, 2015.

Ohno, P. E., Qin, Y. M., Ye, J. H., Wang, J. F., Bertram, A. K., and Martin, S. T.: Fluorescence Aerosol Flow Tube Spectroscopy to Detect Liquid-Liquid Phase Separation, ACS Earth Space Chem., 5, 1223–1232, https://doi.org/10.1021/acsearthspacechem.1c00061, 2021.

Ohno, P. E., Brandao, L., Rainone, E. M., Aruffo, E., Wang, J. F., Qin, Y. M., and Martin, S. T.: Size Dependence of Liquid-Liquid Phase Separation by in Situ Study of Flowing Submicron Aerosol Particles, J. Phys. Chem. A, 127, 2967–2974, https://doi.org/10.1021/acs.jpca.2c08224, 2023.

Onasch, T. B., Siefert, R. L., Brooks, S. D., Prenni, A. J., Murray, B., Wilson, M. A., and Tolbert, M. A.: Infrared Spectroscopic Study of The Deliquescence and Efflorescence of Ammonium Sulfate Aerosol as a Function of Temperature, J. Geophys. Res.-Atmos., 104, 21317–21326, https://doi.org/10.1029/1999jd900384, 1999.

Ott, E. J. E. and Freedman, M. A.: Influence of Ions on the Size Dependent Morphology of Aerosol Particles, ACS Earth Space Chem., 5, 2320–2328, https://doi.org/10.1021/acsearthspacechem.1c00210, 2021.

Ott, E. J. E., Kucinski, T. M., Dawson, J. N., and Freedman, M. A.: Use of Transmission Electron Microscopy for Analysis of Aerosol Particles and Strategies for Imaging Fragile Particles, Anal. Chem., 93, 11347–11356, https://doi.org/10.1021/acs.analchem.0c05225, 2021.

Peng, C., Chan, M. N., and Chan, C. K.: The Hygroscopic Properties of Dicarboxylic and Multifunctional Acids: Measurements and UNIFAC Predictions, Environ. Sci. Technol., 35, 4495–4501, https://doi.org/10.1021/es0107531, 2001.

Peng, C., Jing, B., Guo, Y. C., Zhang, Y. H., and Ge, M. F.: Hygroscopic Behavior of Multicomponent Aerosols Involving NaCl and Dicarboxylic Acids, J. Phys. Chem. A, 120, 1029–1038, https://doi.org/10.1021/acs.jpca.5b09373, 2016.

Peng, C., Chen, L., and Tang, M.: A Database for Deliquescence and Efflorescence Relative Humidities of Compounds with Atmospheric Relevance, Fundam. Res., 2, 578–587, https://doi.org/10.1016/j.fmre.2021.11.021, 2022.

Petters, M. D. and Kreidenweis, S. M.: A single parameter representation of hygroscopic growth and cloud condensation nucleus activity, Atmos. Chem. Phys., 7, 1961–1971, https://doi.org/10.5194/acp-7-1961-2007, 2007.

Pöhlker, C., Saturno, J., Krüger, M. L., Förster, J. D., Weigand, M., Wiedemann, K. T., Bechtel, M., Artaxo, P., and Andreae, M. O.: Efflorescence upon Humidification? X-ray Microspectroscopic in situ Observation of Changes in Aerosol Microstructure and Phase State upon Hydration, Geophys. Res. Lett., 41, 3681–3689, https://doi.org/10.1002/2014gl059409, 2014.

Pöschl, U.: Atmospheric Aerosols: Composition, Transformation, Climate and Health Effects, Angew. Chem. Int. Ed., 44, 7520–7540, https://doi.org/10.1002/anie.200501122, 2005.

Posfai, M., Axisa, D., Tompa, E., Freney, E., Bruintjes, R., and Buseck, P. R.: Interactions of Mineral Dust with Pollution and Clouds: An Individual-Particle TEM Study of Atmospheric Aerosol from Saudi Arabia, Atmos. Res., 122, 347–361, https://doi.org/10.1016/j.atmosres.2012.12.001, 2013.

Pye, H. O. T., Murphy, B. N., Xu, L., Ng, N. L., Carlton, A. G., Guo, H. Y., Weber, R., Vasilakos, P., Appel, K. W., Budisulistiorini, S. H., Surratt, J. D., Nenes, A., Hu, W. W., Jimenez, J. L., Isaacman-VanWertz, G., Misztal, P. K., and Goldstein, A. H.: On the implications of aerosol liquid water and phase separation for organic aerosol mass, Atmos. Chem. Phys., 17, 343–369, https://doi.org/10.5194/acp-17-343-2017, 2017.

Reed, N. W., Wing, B. A., Tolbert, M. A., and Browne, E. C.: Trace $H_2S$ Promotes Organic Aerosol Production and Organosulfur Compound Formation in Archean Analog Haze Photochemistry Experiments, Geophys. Res. Lett., 49, e2021GL097032, https://doi.org/10.1029/2021GL097032, 2022.

Riemer, N., Ault, A. P., West, M., Craig, R. L., and Curtis, J. H.: Aerosol Mixing State: Measurements, Modeling, and Impacts, Rev. Geophys., 57, 187–249, https://doi.org/10.1029/2018rg000615, 2019.

Römpp, A., Winterhalter, R., and Moortgat, G. K.: Oxodicarboxylic acids in atmospheric aerosol particles, Atmos. Environ., 40, 6846–6862, https://doi.org/10.1016/j.atmosenv.2006.05.053, 2006.

Roy, P., Mael, L. E., Makhnenko, I., Martz, R., Grassian, V. H., and Dutcher, C. S.: Temperature-Dependent Phase Transitions of Aqueous Aerosol Droplet Systems in Microfluidic Traps, ACS Earth Space Chem., 4, 1527–1539, https://doi.org/10.1021/acsearthspacechem.0c00114, 2020.

Ruehl, C. R. and Wilson, K. R.: Surface Organic Monolayers Control the Hygroscopic Growth of Submicrometer Particles at High Relative Humidity, J. Phys. Chem. A, 118, 3952–3966, https://doi.org/10.1021/jp502844g, 2014.

Ruehl, C. R., Davies, J. F., and Wilson, K. R.: An Interfacial Mechanism for Cloud Droplet Formation on Organic Aerosols, Science, 351, 1447–1450, https://doi.org/10.1126/science.aad4889, 2016.

Shiraiwa, M., Zuend, A., Bertram, A. K., and Seinfeld, J. H.: Gas-Particle Partitioning of Atmospheric Aerosols: Interplay of Physical State, Non-Ideal Mixing and Morphology, Phys. Chem. Chem. Phys., 15, 11441–11453, https://doi.org/10.1039/c3cp51595h, 2013.

Song, M., Marcolli, C., Krieger, U. K., Zuend, A., and Peter, T.: Liquid-Liquid Phase Separation and Morphology of Internally Mixed Dicarboxylic Acids/Ammonium Sulfate/Water Particles, Atmos. Chem. Phys., 12, 2691–2712, https://doi.org/10.5194/acp-12-2691-2012, 2012a.

Song, M., Marcolli, C., Krieger, U. K., Zuend, A., and Peter, T.: Liquid-Liquid Phase Separation in Aerosol Particles: Dependence on O : C, Organic Functionalities, and Compositional Complexity, Geophys. Res. Lett., 39, L19801, https://doi.org/10.1029/2012gl052807, 2012b.

Song, M., Maclean, A. M., Huang, Y. Z., Smith, N. R., Blair, S. L., Laskin, J., Laskin, A., DeRieux, W. S. W., Li, Y., Shiraiwa, M., Nizkorodov, S. A., and Bertram, A. K.: Liquid-Liquid Phase Separation and Viscosity within Secondary Organic Aerosol Generated from Diesel Fuel Vapors, Atmos. Chem. Phys., 19, 12515–12529, https://doi.org/10.5194/acp-19-12515-2019, 2019.

Song, M. J., Liu, P. F., Martin, S. T., and Bertram, A. K.: Liquid-Liquid Phase Separation in Particles Containing Secondary Organic Material Free of Inorganic Salts, Atmos. Chem. Phys., 17, 11261–11271, https://doi.org/10.5194/acp-17-11261-2017, 2017.

Stewart, D. J., Cai, C., Nayler, J., Preston, T. C., Reid, J. P., Krieger, U. K., Marcolli, C., and Zhang, Y. H.: Liquid-Liquid Phase Separation in Mixed Organic/Inorganic Single Aqueous Aerosol Droplets, J. Phys. Chem. A, 119, 4177–4190, https://doi.org/10.1021/acs.jpca.5b01658, 2015.

Takahama, S., Pathak, R. K., and Pandis, S. N.: Efflorescence Transitions of Ammonium Sulfate Particles Coated with Secondary Organic Aerosol, Environ. Sci. Technol., 41, 2289–2295, https://doi.org/10.1021/es0619915, 2007.

Ting, Y. C., Mitchell, E. J. S., Allan, J. D., Liu, D. T., Spracklen, D. V., Williams, A., Jones, J. M., Lea-Langton, A. R., McFiggans, G., and Coe, H.: Mixing State of Carbonaceous Aerosols of Primary Emissions from "Improved" African Cookstoves, Environ. Sci. Technol., 52, 10134–10143, https://doi.org/10.1021/acs.est.8b00456, 2018.

Tolocka, M. P. and Turpin, B.: Contribution of Organosulfur Compounds to Organic Aerosol Mass, Environ. Sci. Technol., 46, 7978–7983, https://doi.org/10.1021/es300651v, 2012.

Tong, Y. K., Meng, X. X. Y., Zhou, B., Sun, R., Wu, Z. J., Hu, M., and Ye, A. P.: Detecting the pH-dependent liquid-liquid phase separation of single levitated aerosol microdroplets via laser tweezers-Raman spectroscopy, Front. Phys., 10, 969921, https://doi.org/10.3389/fphy.2022.969921, 2022.

Unga, F., Choel, M., Derimian, Y., Deboudt, K., Dubovik, O., and Goloub, P.: Microscopic Observations of Core-Shell Particle Structure and Implications for Atmospheric Aerosol Remote Sensing, J. Geophys. Res.-Atmos., 123, 13944–13962, https://doi.org/10.1029/2018jd028602, 2018.

Veghte, D. P., Bittner, D. R., and Freedman, M. A.: Cryo-Transmission Electron Microscopy Imaging of the Morphology of Submicrometer Aerosol Containing Organic Acids and Ammonium Sulfate, Anal. Chem., 86, 2436–2442, https://doi.org/10.1021/ac403279f, 2014.

Voorhees, P. W.: The Theory of Ostwald Ripening, J. Stat. Phys., 38, 231–252, https://doi.org/10.1007/Bf01017860, 1985.

Wang, N., Jing, B., Wang, P., Wang, Z., Li, J. R., Pang, S. F., Zhang, Y. H., and Ge, M. F.: Hygroscopicity and Compositional Evolution of Atmospheric Aerosols Containing Water-Soluble Carboxylic Acid Salts and Ammonium Sulfate: Influence of Ammonium Depletion, Environ. Sci. Technol., 53, 6225–6234, https://doi.org/10.1021/acs.est.8b07052, 2019.

Wang, W. H., Shao, L. Y., Mazzoleni, C., Li, Y. W., Kotthaus, S., Grimmond, S., Bhandari, J., Xing, J. P., Feng, X. L., Zhang, M. Y., and Shi, Z. B.: Measurement report: Comparison of wintertime individual particles at ground level and above the mixed layer in urban Beijing, Atmos. Chem. Phys., 21, 5301–5314, https://doi.org/10.5194/acp-21-5301-2021, 2021.

Wise, M. E., Martin, S. T., Russell, L. M., and Buseck, P. R.: Water Uptake by NaCl Particles Prior to Deliquescence and the Phase Rule, Aerosol Sci. Tech., 42, 281–294, https://doi.org/10.1080/02786820802047115, 2008.

Xiong, C., Chen, X. Y., Ding, X. L., Kuang, B. Y., Pei, X. Y., Xu, Z. N., Yang, S. K., Hu, H., and Wang, Z. B.: Reconsideration of Surface Tension and Phase State Effects on Cloud Condensation Nuclei Activity Based on the Atomic Force Microscopy Measurement, Atmos. Chem. Phys., 22, 16123–16135, https://doi.org/10.5194/acp-22-16123-2022, 2022.

Xiong, C., Kuang, B. Y., Zhang, F., Pei, X. Y., Xu, Z. N., and Wang, Z. B.: In-situ observation for RH-dependent mixing states of submicron particles containing organic surfactants and inorganic salts, Zenodo [data set], https://doi.org/10.5281/zenodo.8079001, 2023.

Xu, L., Fukushima, S., Sobanska, S., Murata, K., Naganuma, A., Liu, L., Wang, Y. Y., Niu, H. Y., Shi, Z. B., Kojima, T., Zhang, D. Z., and Li, W. J.: Tracing the evolution of morphology and mixing state of soot particles along with the movement of an Asian dust storm, Atmos. Chem. Phys., 20, 14321–14332, https://doi.org/10.5194/acp-20-14321-2020, 2020.

Xu, W. Q., Chen, C., Qiu, Y. M., Li, Y., Zhang, Z. Q., Karnezi, E., Pandis, S. N., Xie, C. H., Li, Z. J., Sun, J. X., Ma, N., Xu, W. Y., Fu, P. Q., Wang, Z. F., Zhu, J., Worsnop, D. R., Ng, N. L., and Sun, Y. L.: Organic aerosol volatility and viscosity in the North China Plain: contrast between summer and winter, Atmos. Chem. Phys., 21, 5463–5476, https://doi.org/10.5194/acp-21-5463-2021, 2021.

Yang, H., Wang, N., Pang, S. F., Zheng, C. M., and Zhang, Y. H.: Chemical reaction between sodium pyruvate and ammonium sulfate in aerosol particles and resultant sodium sulfate efflorescence, Chemosphere, 215, 554–562, https://doi.org/10.1016/j.chemosphere.2018.10.062, 2019.

You, Y. and Bertram, A. K.: Effects of Molecular Weight and Temperature on Liquid-Liquid Phase Separation in Particles Containing Organic Species and Inorganic Salts, Atmos. Chem. Phys., 15, 1351–1365, https://doi.org/10.5194/acp-15-1351-2015, 2015.

You, Y., Renbaum-Wolff, L., Carreras-Sospedra, M., Hanna, S. J., Hiranuma, N., Kamal, S., Smith, M. L., Zhang, X. L., Weber, R. J., Shilling, J. E., Dabdub, D., Martin, S. T., and Bertram, A. K.: Images Reveal that Atmospheric Particles can Undergo Liquid-Liquid Phase Separations, P. Natl. Acad. Sci. USA, 109, 13188–13193, https://doi.org/10.1073/pnas.1206414109, 2012.

You, Y., Renbaum-Wolff, L., and Bertram, A. K.: Liquid–liquid phase separation in particles containing organics mixed with ammonium sulfate, ammonium bisulfate, ammonium nitrate or sodium chloride, Atmos. Chem. Phys., 13, 11723–11734, https://doi.org/10.5194/acp-13-11723-2013, 2013.

Závacká, K., Nedvela, V., Olbert, M., Tihlaříková, E., Vetráková, L., Yang, X., and Heger, D.: Temperature and Concentration Affect Particle Size Upon Sublimation Saline Ice: Implications for Sea Salt Aerosol Production in Polar Regions, Geophys. Res. Lett., 49, e2021GL097098, https://doi.org/10.1029/2021GL097098, 2022.

Zaveri, R. A., Easter, R. C., Fast, J. D., and Peters, L. K.: Model for Simulating Aerosol Interactions and Chemistry (MOSAIC), J. Geophys. Res.-Atmos., 113, D13204, https://doi.org/10.1029/2007jd008782, 2008.

Zeng, G., Kelley, J., Kish, J. D., and Liu, Y.: Temperature-Dependent Deliquescent and Efflorescent Properties of Methanesulfonate Sodium Studied by ATR-FTIR Spectroscopy, J. Phys. Chem. A, 118, 583–591, https://doi.org/10.1021/jp405896y, 2014.

Zhang, J., Yuan, Q., Liu, L., Wang, Y. Y., Zhang, Y. X., Xu, L., Pang, Y., Zhu, Y. H., Niu, H. Y., Shao, L. Y., Yang, S. S., Liu, H., Pan, X. L., Shi, Z. B., Hu, M., Fu, P. Q., and Li, W. J.: Trans-Regional Transport of Haze Particles From the North China Plain to Yangtze River Delta During Winter, J. Geophys. Res.-Atmos., 126, e2020JD033778, https://doi.org/10.1029/2020JD033778, 2021.

Zhang, J., Wang, Y. Y., Teng, X. M., Liu, L., Xu, Y. S., Ren, L. H., Shi, Z. B., Zhang, Y., Jiang, J. K., Liu, D. T., Hu, M., Shao, L. Y., Chen, J. M., Martin, S. T., Zhang, X. Y., and Li, W. J.: Liquid-Liquid Phase Separation Reduces Radiative Absorption by Aged Black Carbon Aerosols, Commun. Earth Environ., 3, 128, https://doi.org/10.1038/s43247-022-00462-1, 2022.

Zhang, Y., Chen, Y. Z., Lambe, A. T., Olson, N. E., Lei, Z. Y., Craig, R. L., Zhang, Z. F., Gold, A., Onasch, T. B., Jayne, J. T., Worsnop, D. R., Gaston, C. J., Thornton, J. A., Vizuete, W., Ault, A. P., and Surratt, J. D.: Effect of the Aerosol-Phase State on Secondary Organic Aerosol Formation from the Reactive Uptake of Isoprene-Derived Epoxydiols (IEPDX), Environ. Sci. Technol. Lett., 5, 167–174, https://doi.org/10.1021/acs.estlett.8b00044, 2018.

Zhang, Y. X., Zhang, Q., Yao, Z. L., and Li, H. Y.: Particle Size and Mixing State of Freshly Emitted Black Carbon from Different Combustion Sources in China, Environ. Sci. Technol., 54, 7766–7774, https://doi.org/10.1021/acs.est.9b07373, 2020.

Zhu, Y., Pang, S., and Zhang, Y.: Observations on the unique phase transitions of inorganics relevant due to gluconic acid in particles, Atmos. Environ., 288, 119313, https://doi.org/10.1016/j.atmosenv.2022.119313, 2022.